Formaldehyde columns from the Ozone Monitoring Instrument: Urban versus background levels and evaluation using aircraft data and a global model

Nicholas L. Boeke,[1] Julian D. Marshall,[1] Sergio Alvarez,[2] Kelly V. Chance,[3] Alan Fried,[4] Thomas P. Kurosu,[3] Bernhard Rappenglück,[2] Dirk Richter,[4] James Walega,[4] Petter Weibring,[4] and Dylan B. Millet[1,5]

Received 5 August 2010; revised 19 November 2010; accepted 13 December 2010; published 10 March 2011.

[1] We combine aircraft measurements (Second Texas Air Quality Study, Megacity Initiative: Local and Global Research Observations, Intercontinental Chemical Transport Experiment: Phase B) over the United States, Mexico, and the Pacific with a 3-D model (GEOS-Chem) to evaluate formaldehyde column (Ω_{HCHO}) retrievals from the Ozone Monitoring Instrument (OMI) and assess the information they provide on HCHO across local to regional scales and urban to background regimes. OMI Ω_{HCHO} correlates well with columns derived from aircraft measurements and GEOS-Chem (R = 0.80). For the full data ensemble, OMI's mean bias is −3% relative to aircraft-derived Ω_{HCHO} (−17% where $\Omega_{HCHO} > 5 \times 10^{15}$ molecules cm^{-2}) and −8% relative to GEOS-Chem, within expected uncertainty for the retrieval. Some negative bias is expected for the satellite and model, given the plume sampling of many flights and averaging over the satellite and model footprints. Major axis regression for OMI versus aircraft and model columns yields slopes (95% confidence intervals) of 0.80 (0.62–1.03) and 0.98 (0.73–1.35), respectively, with no significant intercept. Aircraft measurements indicate that the normalized vertical HCHO distribution, required by the satellite retrieval, is well captured by GEOS-Chem, except near Mexico City. Using measured HCHO profiles in the retrieval algorithm does not improve satellite-aircraft agreement, suggesting that use of a global model to specify shape factors does not substantially degrade retrievals over polluted areas. While the OMI measurements show that biogenic volatile organic compounds dominate intra-annual and regional Ω_{HCHO} variability across the United States, smaller anthropogenic Ω_{HCHO} gradients are detectable at finer spatial scales (~20–200 km) near many urban areas.

Citation: Boeke, N. L., et al. (2011), Formaldehyde columns from the Ozone Monitoring Instrument: Urban versus background levels and evaluation using aircraft data and a global model, *J. Geophys. Res.*, *116*, D05303, doi:10.1029/2010JD014870.

1. Introduction

[2] Formaldehyde (HCHO) is a common product in the oxidation of atmospheric volatile organic compounds (VOCs), with a typical lifetime (against photolysis and oxidation by OH) of a few hours in daytime [*Sander et al.*, 2006]. While methane oxidation is the largest HCHO source to the global troposphere, HCHO variability over land is dominated by its production from nonmethane VOCs [*Millet et al.*, 2006; *Stavrakou et al.*, 2009b]. Primary HCHO emissions from combustion [*Garcia et al.*, 2006] and vegetation [*Janson et al.*, 1999; *Kesselmeier and Staudt*, 1999; *Martin et al.*, 1999; *Seco et al.*, 2007] also contribute but are minor compared to secondary formation. Measurements of HCHO columns (Ω_{HCHO}, molecules cm^{-2}) from the Ozone Monitoring Instrument (OMI) and other space-borne sensors can provide local-to-global constraints on the emission sources and photochemical processing of VOCs [*Chance et al.*, 2000; *Abbot et al.*, 2003; *Palmer et al.*, 2003, 2006, 2007; *Wittrock et al.*, 2006; *Millet et al.*, 2006, 2008; *Fu et al.*, 2007; *Stavrakou et al.*, 2009a; *Duncan et al.*, 2010; *Curci et al.*, 2010]. Here we combine OMI Ω_{HCHO} data, aircraft measurements (collected over the United States, Mexico and the Pacific Ocean) and a chemical transport model (GEOS-Chem) to evaluate OMI measure-

[1]Department of Civil Engineering, University of Minnesota, Minneapolis, Minnesota, USA.
[2]Department of Earth and Atmospheric Sciences, University of Houston, Houston, Texas, USA.
[3]Atomic and Molecular Physics Division, Harvard-Smithsonian Center for Astrophysics, Cambridge, Massachusetts, USA.
[4]Earth Observing Laboratory, National Center for Atmospheric Research, Boulder, Colorado, USA.
[5]Department of Soil, Water, and Climate, University of Minnesota, St. Paul, Minnesota, USA.

0148-0227/11/2010JD014870

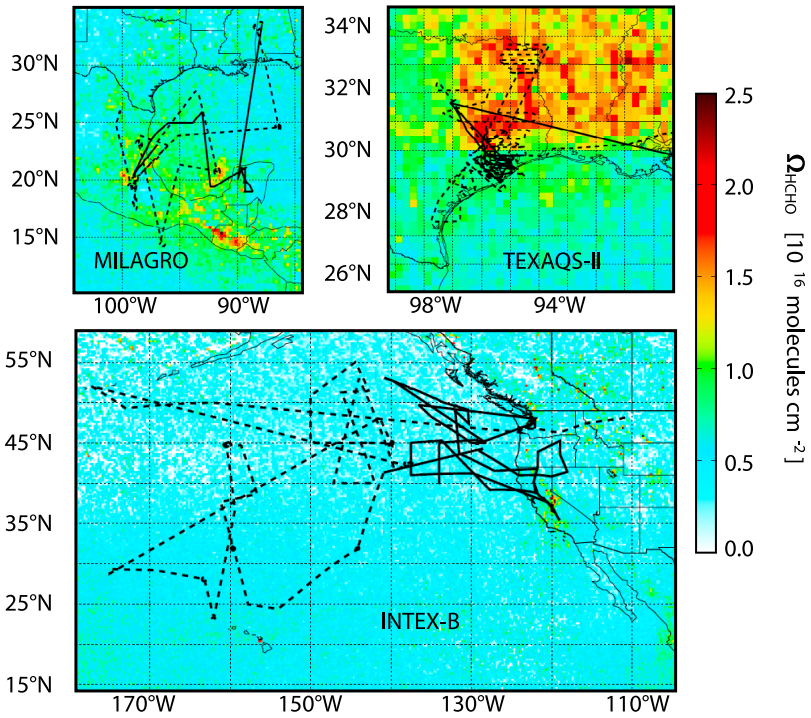

Figure 1. Flight track segments (1200–1500 LT) used for cross-comparison with the Ozone Monitoring Instrument (OMI) and GEOS-Chem (Megacity Initiative: Local and Global Research Observations and Intercontinental Chemical Transport Experiment: Phase B, solid line = C-130, dashed line = DC-8; Second Texas Air Quality Study, solid line = Piper Aztec, dashed line = WP-3D). Tracks are mapped over the campaign-mean HCHO column abundance (0.25° × 0.25° grid), as measured by OMI.

ments and assess the information they provide on HCHO in urban versus background regimes.

[3] Space-borne sensors for measuring atmospheric HCHO include the Global Ozone Monitoring Experiment (GOME-1 [*Burrows et al.*, 1999; *Chance et al.*, 2000] and GOME-2 [*Callies et al.*, 2000]), the Scanning Imaging Absorption Spectrometer for Atmospheric Chartography (SCIAMACHY) [*Burrows et al.*, 1995; *Bovensmann et al.*, 1999], and OMI [*Levelt et al.*, 2006]. In each case Ω_{HCHO} is determined from solar backscatter measurements in near-UV wavelengths (310–365 nm). Of the available sensors, OMI's high spatial resolution (13 × 24 km^2 at nadir) and daily global coverage offer substantial advantages for resolving spatial variability and reducing measurement uncertainty through improved sampling statistics. The small footprint also reduces data contamination by clouds, the primary source of error in the retrieval [*Millet et al.*, 2006].

[4] Research to date has applied HCHO column data to study anthropogenic and biogenic VOC emissions from North and South America [*Abbot et al.*, 2003; *Palmer et al.*, 2003, 2006, 2007; *Barkley et al.*, 2008; *Millet et al.*, 2006, 2008], Europe [*Dufour et al.*, 2009; *Curci et al.*, 2010], Asia [*Fu et al.*, 2007], and the globe [*Wittrock et al.*, 2006; *Stavrakou et al.*, 2009a, 2009b; *Shim et al.*, 2005], and to examine ozone chemistry over the United States [*Martin et al.*, 2004b; *Duncan et al.*, 2010]. Quantitative interpretation of Ω_{HCHO} retrievals requires error characterization and consistency evaluation against other data sets, but opportunities for direct validation have so far been limited, particularly for OMI. *Millet et al.* [2008] compared OMI Ω_{HCHO} with GOME-1 and found differences of 2%–14% (with OMI lower), less than the estimated measurement uncertainty. Others have compared HCHO retrievals from SCIAMACHY with ground-based UV/visible light and Fourier transform infrared measurements [*Wittrock et al.*, 2006; *Vigouroux et al.*, 2009]. Earlier work by *Ladstätter-Weißenmayer et al.* [2003] and *Martin et al.* [2004a] carried out comparisons between GOME-1 HCHO and some of the limited aircraft measurements then available; both studies found agreement between satellite and in situ measurements within instrument uncertainty, including where Ω_{HCHO} was near the detection limit (4.0×10^{15} molecules cm^{-2}) [*Chance et al.*, 2000].

[5] Here we use aircraft measurements (collected over the United States, Mexico and the Pacific Ocean) and a chemical transport model (GEOS-Chem) to evaluate and interpret OMI Ω_{HCHO} measurements. The present analysis builds on previous work by directly evaluating OMI Ω_{HCHO} and its variability across marine to urban regimes. We then apply the OMI data to examine HCHO gradients over North America across urban-to-background regimes as a function of season. We interpret our findings with respect to their implications for uncertainty in Ω_{HCHO} retrievals from OMI and similar space-borne sensors.

2. Data Sources

2.1. Aircraft Campaigns

[6] Figure 1 shows flight tracks for the aircraft campaigns used here: the Second Texas Air Quality Study (TexAQS II)

Table 1. Aircraft Campaigns Used for OMI Evaluation

Campaign	Platform	Total Flights[a]	Flight Dates (2006)	Region	Measurement Technique[b]	Measurement Reference
TexAQS II	Aztec	11 (2)	21 Aug–5 Oct	Houston, Texas	FHR	*Rappenglück et al.* [2010]
TexAQS II	WP-3D	18 (6)	31 Aug–13 Sep	Houston, Texas, and surrounding area	DFGAS	*Weibring et al.* [2007]
MILAGRO	C-130	13 (1)	4–31 Mar	Vera Cruz to Mexico City; Gulf of Mexico to Texas	DFGAS	*Weibring et al.* [2007]
MILAGRO	DC-8	7 (5)	4–22 Mar	Houston, Texas, to Mexico City; Sierra Madre Mountains	TDLAS	*Fried et al.* [2010]
INTEX-B	C-130	12 (9)	17 Apr–15 May	Pacific Northwest	DFGAS	*Weibring et al.* [2007]
INTEX-B	DC-8	10 (6)	17 Apr–15 May	north central and South Pacific; Hawaii to Alaska	TDLAS	*Fried et al.* [2010]

[a]Parentheses indicate the number of flights retained from each campaign for comparison to OMI.
[b]Abbreviations are as follows: FHR, fluorometric Hantzsch reaction spectroscopy; DFGAS, difference frequency generation absorption spectrometry; TDLAS, tunable diode laser absorption spectroscopy.

[*Parrish et al.*, 2009], the Megacity Initiative: Local and Global Research Observations (MILAGRO) [*Molina et al.*, 2010], and the Intercontinental Chemical Transport Experiment: Phase B (INTEX-B) [*Singh et al.*, 2009]. Table 1 summarizes the spatial domain, time frame, and HCHO measurement techniques used during each campaign.

[7] The 2006 TexAQS II campaign focused on understanding emissions, chemical processing, and air quality in Texas air sheds. We use data from the NOAA WP-3D Lockheed Orion (flight ceiling 8600 m) and the Baylor University Piper Aztec (flight ceiling 6100 m) deployed during TexAQS II, both based out of Houston. HCHO mixing ratios were measured by the National Center for Atmospheric Research (NCAR) aboard the WP-3D by difference frequency generation absorption spectrometry (DFGAS) with an uncertainty of 13% and limit of detection (LOD) of 20–30 pptv (1σ, 30 s averaging) [*Weibring et al.*, 2007]. The University of Houston measured HCHO aboard the Piper Aztec by fluorometric Hantzsch reaction (FHR) with an LOD of 50–120 pptv (1 min averaging) and uncertainty of 10% [*Rappenglück et al.*, 2010].

[8] The MILAGRO/INTEX-B campaigns were aimed at understanding air pollution transport from Mexico City and Asia and the associated climatic effects. We use HCHO data collected by NCAR on board the C-130 and DC-8 aircraft deployed during these campaigns. The C-130 was outfitted with the DFGAS instrumentation described above. During MILAGRO the LOD ranged between 35 and 55 pptv (1σ, 30 s averaging), which improved to 20–30 pptv (30 s averaging) during INTEX-B. The DC-8 measurements employed tunable diode laser absorption spectroscopy (TDLAS) with an LOD of 20–30 pptv (1σ, 1 min averaging) and uncertainty of 13–15% (A. Fried et al., manuscript in preparation, 2010). The C-130 was based out of Seattle during INTEX-B and Vera Cruz, Mexico during MILAGRO. The DC-8 was based out of Honolulu and Anchorage during INTEX-B, and Houston during MILAGRO.

2.2. Ozone Monitoring Instrument

[9] OMI is on board NASA's EOS Aura satellite at ~705 km altitude in a Sun-synchronous orbit with 98° inclination and 1338 local equator crossing time [*Levelt et al.*, 2006]. Aura's period is approximately 99 min, providing 14 to 15 orbits and global coverage daily. OMI is a UV/visible light nadir solar backscatter CCD spectrometer covering the spectral range 270–500 nm with a resolution of 0.45 nm between 310 and 365 nm. OMI has a 114° swath angle covering approximately 2600 km on Earth; its 60 pixels have footprints ranging from 13×24 km^2 at nadir to 28×160 km^2 at swath edges. OMI reads out a single cross-track swath line approximately every 3.5 s yielding 1644 swaths per orbit.

[10] For our analysis we use the standard OMI HCHO data product version 2.0 (Collection 3). Column values are subject to a number of quality checks. Aside from cloud screening (see below), only column values flagged as "good" in the product are included [*Kurosu*, 2008]. Across-track striping (discontinuities across the swath), arising from imperfect cross-calibration and different dead/hot pixel masks for the 60 CCD detector regions that provide the across-track coverage, has a significant effect on HCHO due to the small atmospheric optical density of this absorber. The derivation of the OMI HCHO data product includes methods to minimize this effect, including use of an earthshine radiance from the remote Pacific in lieu of a solar irradiance reference, residual outlier screening during the nonlinear least squares fitting procedure, and the application of a postretrieval across-track smoothing filter. Temporal averaging over longer time periods further removes the impact of the stripes. During June 2007 OMI developed an anomaly affecting radiance measurements in cross-track positions 53 and 54 (0-based) caused by a partial external blockage of the radiance port. This so-called row anomaly expanded over time to other cross-track positions and is being actively monitored by the instrument team (http://www.knmi.nl/omi/research/product/rowanomaly-background.php). We remove these pixels from consideration in all postanomaly orbits.

[11] For comparing OMI with the aircraft data we restrict flight data to times bracketing the OMI nadir overpass (1200–1500 LT), a criterion that excludes 33 of 71 total flights (Figure 1). We also restrict the use of OMI pixels to those at solar zenith angle (SZA) $\leq 80°$ (see http://eospso.gsfc.nasa.gov/eos_homepage/for_scientists/atbd/viewInstrument.php?instrument = 13/) and cloud fraction ≤ 0.4 [*Chance et al.*, 2000; *Palmer et al.*, 2001; *Millet et al.*, 2006], eliminating OMI retrievals during 7 of the 38 remaining flights.

2.3. GEOS-Chem Chemical Transport Model

[12] We use the GEOS-Chem 3-D model of atmospheric chemistry to simulate Ω_{HCHO} for cross-evaluation with OMI and the aircraft data, and to specify the HCHO vertical profile shapes needed in the OMI retrieval (see section 3.1).

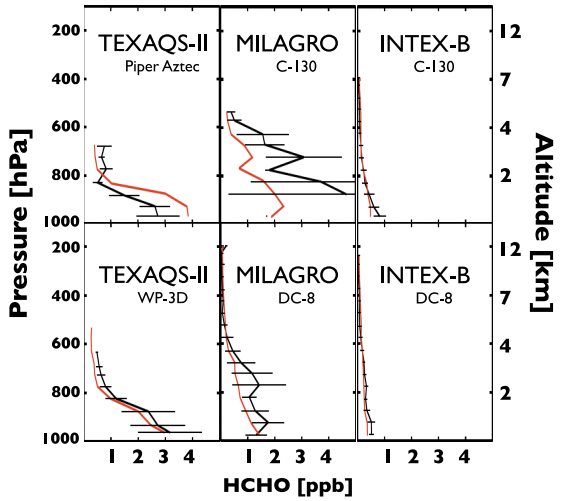

Figure 2. HCHO mixing ratios measured (black) and simulated by GEOS-Chem (red) averaged vertically in 50 hPa bins for each campaign and platform. Error bars show the bin standard deviation for measured HCHO.

GEOS-Chem v8.2 (http://www.GEOS-Chem.org/) is a 3-D Eulerian global chemical transport model including detailed ozone-NO_x-VOC chemistry [*Bey et al.*, 2001]. The chemical mechanism includes >80 species and >300 reactions including heterogeneous chemistry, with aerosols simulated as described by *Park et al.* [2004]. GEOS-Chem uses assimilated meteorological data from the NASA Goddard Earth Observing System (GEOS-5) including mixing height and surface characteristics (3 hour temporal resolution), wind, convective and advective mass transport, clouds, temperature and precipitation (6 hour resolution) [*Bey et al.*, 2001; *Park et al.*, 2004]. The meteorological data have 0.5° × 0.667° spatial resolution (latitude × longitude) and 72 vertical layers, which we degrade to 2° × 2.5° and 47 vertical layers for computational expediency. Anthropogenic and biogenic emissions used here are described elsewhere [*Millet et al.*, 2010]. For consistency with the aircraft data we sample the model along each flight track at the time and location of the in situ measurements and calculate HCHO columns as described in section 3.

3. HCHO Column Determination

3.1. OMI HCHO Column Retrievals

[13] HCHO column abundance is retrieved from OMI observations of solar radiation backscattered and reflected from Earth's atmosphere and surface. Radiances are processed through spectral fitting algorithms in the 327.5–356.5 nm window based on nonlinear least squares minimization to retrieve the HCHO abundance along the viewing path (slant column). The ratio of the slant column to the vertical column amount (air mass factor, AMF) is a function of viewing geometry, surface reflectance, atmospheric scattering, and the normalized vertical distribution of HCHO (shape factor) [*Palmer et al.*, 2001]. Here we compute AMFs with a lookup table derived using the Doubling Adding KNMI (DAK) radiative transfer model [*Stammes*, 2001]. In calculating the AMF for each OMI pixel we use GEOS-Chem to estimate the HCHO shape factor at the location and time of the satellite overpass. This approach assures self-consistency when comparing retrieved columns to those simulated by GEOS-Chem but may introduce model bias in the retrieval, as discussed below. Sources of error in the AMF, in addition to the specification of the shape factor, include cloud and aerosol effects and the surface albedo. In previous work, *Millet et al.* [2006] found the combination of these to result in an overall AMF uncertainty of <20% for a scene with a cloud fraction of 0.2.

[14] The spectral fitting uncertainty for OMI HCHO slant columns ranges from 40% to 100%, comparable to the instrument's predecessors, though this uncertainty can be significantly reduced through the increased sampling made possible by OMI's small footprint and high temporal coverage. For comparison with aircraft data we average all OMI pixels transected by a flight track. This approach reduces the effective spatial resolution, particularly for long flight tracks, but also reduces random error in the comparisons. The number of OMI observations averaged together for any given flight ranges from 7 to 199 (median = 69) resulting in an average uncertainty for all flights of 29% (relative standard error of all OMI scenes) or 15% where $\Omega_{HCHO} > 5.0 \times 10^{15}$ molecules cm^{-2}.

3.2. HCHO Vertical Profiles and Columns Computed From Aircraft Measurements and GEOS-Chem

[15] Figure 2 compares mean HCHO vertical profiles measured aboard the aircraft (averaged in 50 hPa bins) to those simulated by GEOS-Chem for each of the aircraft campaigns. The ordinate value of each data point is determined as the average altitude of all HCHO measurements in each bin. Over land and in continental outflow (e.g., MILAGRO, TexAQS II) we observe the highest HCHO concentrations near the surface, decreasing strongly with height above the boundary layer. Over the remote ocean (e.g., INTEX-B) we see low concentrations throughout the atmospheric column with little vertical gradient. These patterns reflect the predominant terrestrial source of HCHO precursors combined with the short atmospheric lifetime of HCHO. On average GEOS-Chem captures the observed HCHO profile shape, providing support for its use in computing the AMF. An exception is over and downwind of Mexico City (MILAGRO campaign), where a low model bias is evident compared to highly variable in situ observations. A. Fried et al. (manuscript in preparation, 2010) discuss the potential cause for analogous box model underestimates in this regime.

[16] We estimate Ω_{HCHO} from the observed and modeled profiles on each flight day (1200–1500 LT) by integrating the mean vertical HCHO profile (expressed in number concentration, molecules cm^{-3}) from the flight floor to the flight ceiling. To estimate HCHO abundance above and below each profile, we extrapolate the topmost measured mixing ratio as constant to the tropopause (zero above the tropopause) and the bottommost measured mixing ratio as constant to the surface. The tropopause is taken as the monthly mean GEOS-5 value across the flight domain. Surface altitude is determined from a 10 min resolution topographic map.

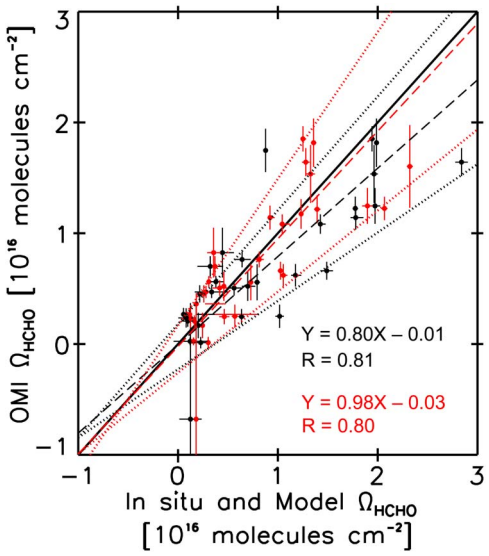

Figure 3. OMI HCHO columns versus model (red) and aircraft (black) profile-derived HCHO columns. Dashed lines are best fit (major axis regression), with regression parameters given in the inset. Dotted lines show the 95% confidence interval for the best-fit line. Vertical error bars show the standard error in the OMI column values, and horizontal error bars show the estimated uncertainty in each profile-derived column.

[17] The mean flight floor across flights ranges from 308 to 532 m for the various campaigns. During TexAQS II, with its urban focus, the fraction of measurements taken in the boundary layer ranges between 51% and 100% for the two aircraft (versus 14%–59% and 2%–37% for INTEX-B and MILAGRO, respectively). We discard any computed columns where the extrapolated fraction (above and below the measured HCHO profile) exceeds 50% of the total computed HCHO column, leaving a total of 29 flights for the comparison. The GEOS-Chem HCHO columns computed in this way agree well with the average of the full model columns over transected grid squares (weighted by the number of measurements over each) (R = 0.98, slope = 1.10 (0.99–1.21), intercept = −0.02 (−0.08–0.05) (95% confidence interval (CI)), demonstrating the reliability of the overall extrapolation approach.

[18] We estimate the uncertainty in the extrapolated columns by computing upper and lower limits as follows. We recalculate Ω_{HCHO} using the vertical profiles of mean HCHO concentration $\pm1\sigma$ (standard deviation) for each vertical bin and extrapolate using the flight's mean tropopause height and mean surface altitude $\pm1\sigma$. We find in this way that most of the uncertainty in the extrapolated columns stems from HCHO ambient variability over the domain of each flight (on average 67% of total uncertainty), with a smaller error introduced by extrapolating to the surface (20% of total uncertainty) and tropopause (13% of total uncertainty). Over all flights, the uncertainty in the HCHO columns derived in this way ranges from −17% to +17% (mean = 6%), which is similar to the level of agreement between the GEOS-Chem extrapolated and full vertical HCHO columns.

4. Comparing OMI HCHO Columns With Modeled and in Situ Values

[19] Figure 3 compares OMI Ω_{HCHO} with columns derived from the measured and simulated profiles. Note that negative Ω_{HCHO} values can occur in the OMI retrieval as the result of minimizing residuals during the spectral fitting when HCHO is close to or below the sensor detection limit (OMI HCHO columns flagged as "good" and used here are ≥0 within 2σ fitting uncertainties). Discarding those negative values would produce an erroneously high bias in any temporal or spatial averaging. The OMI HCHO columns are well correlated with those derived from the aircraft and model profiles: R = 0.81 (0.68–0.91) and 0.80 (0.75–0.88) (95% CI), respectively. Major axis regression of OMI versus model Ω_{HCHO} yields a best-fit line of Y = 0.98 (0.73–1.35)X − 0.03 (−0.28–0.17) (95% CI). The corresponding fit for OMI versus aircraft columns is Y = 0.80 (0.62–1.03) X − 0.01 (−0.23–0.18) (95% CI). These statistics include only columns with extrapolated fraction <50%. A more restrictive criterion (<20%) yields regressions with very similar slopes and intercepts but reduces the correlation (to 0.69 versus the measurements and 0.79 versus the model).

[20] This data set represents a challenging test case for both the satellite and the model since many flights focused on sampling polluted urban and biomass-burning plumes, which may be diluted by averaging over the satellite/model footprint (up to 28 × 160 km^2 and 2° × 2.5°). Nevertheless, as shown in Figure 4, OMI's relative bias compared to the aircraft columns is less than 3% for the full data ensemble and −17% when HCHO is elevated ($\Omega_{HCHO} > 5 \times 10^{15}$ molecules cm^{-2}), values that are within the expected uncertainty in satellite-based HCHO column measurements [*Millet et al.*, 2006] and comparable to the level of uncertainty in extrapolating full columns from the flight-track data. This bias is also similar to what was found earlier (−2 to −14%) for OMI relative to GOME-1 [*Millet et al.*, 2008]. The average bias

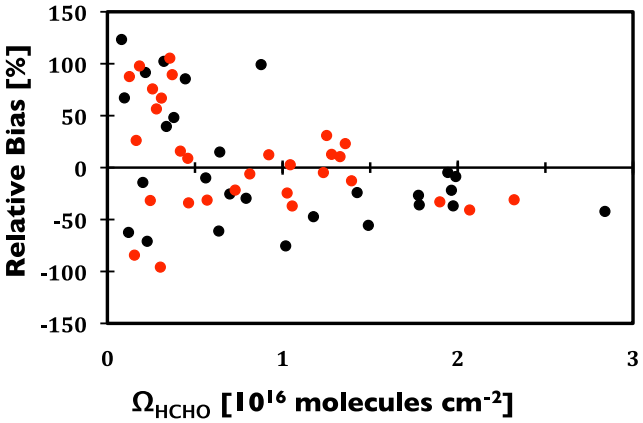

Figure 4. OMI relative bias as a function of HCHO column abundance relative to in situ (black) and modeled (red) columns.

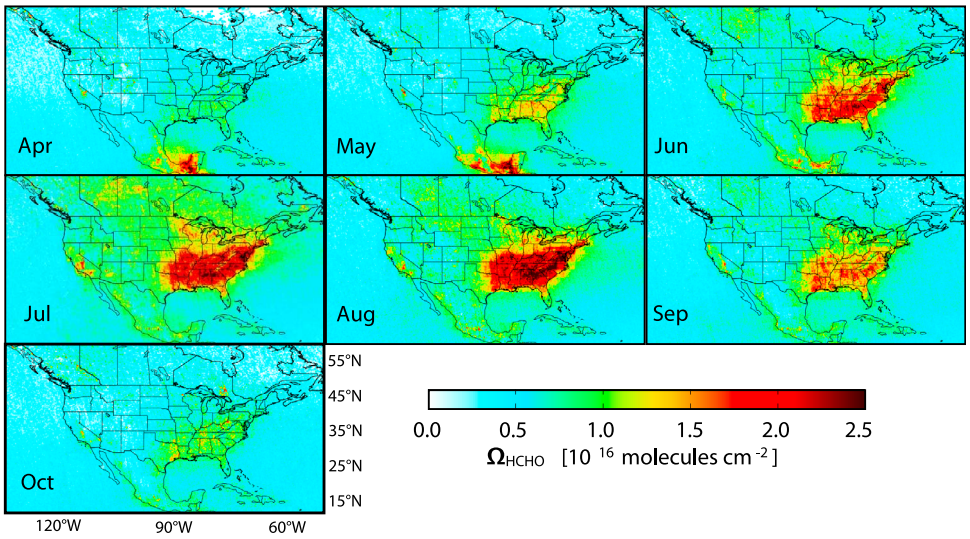

Figure 5. Monthly mean OMI HCHO columns over North America during 2005–2007 (inclusive) gridded to 0.25° × 0.25°. Data are screened for cloud fraction ≤0.4, for solar zenith angle ≤80°, and for statistical outliers.

for the GEOS-Chem columns compared to the aircraft values is −5% for all flights and −23% when $\Omega_{HCHO} > 5 \times 10^{15}$ molecules cm^{-2}.

[21] Computing the AMF in the HCHO retrieval requires a priori the normalized vertical distribution of HCHO (shape factor) for each satellite pixel. This information may be taken from climatology or provided by a 3-D model (here we use GEOS-Chem). To see how this parameter affects the OMI retrievals, we recomputed the AMFs using the measured in situ HCHO profiles for each flight in lieu of the corresponding modeled profiles. AMFs calculated using the measured HCHO profiles were on average 95% ± 15% (1σ) of those calculated using shape factors from GEOS-Chem. The overall level of agreement between OMI and aircraft HCHO columns did not improve with the use of measured HCHO profiles in the retrieval.

5. Temporal and Spatial Gradients in HCHO Over North America as Observed by OMI

[22] In this section we apply the OMI data to investigate spatial and temporal patterns in urban versus rural Ω_{HCHO} across the United States, and the extent to which these patterns are modified by anthropogenic VOCs in a way that is detectable from space.

[23] Figure 5 shows monthly mean OMI Ω_{HCHO} retrievals over North America for April-October during 2005–2007. Individual OMI pixels are projected onto, and averaged over, a 0.25° × 0.25° grid. There is a clear seasonal cycle over North America, especially pronounced in the U.S. Southeast, which is consistent with the distribution of biogenic VOC emissions and changes in solar radiation and temperature during the growing season. Despite significant (albeit declining) anthropogenic VOC emissions in the United States [*Parrish*, 2006] and OMI's high spatial resolution, observed HCHO columns over urban areas generally do not (at any time of year) exhibit the dramatic enhancements seen over the U.S. Southeast during the growing season. Variability in Ω_{HCHO} reflects the emission strength and near-field HCHO yield of precursor VOCs. As seen in Figure 5, the product of the two is dominated by biogenic VOCs over the United States (and in particular by isoprene emissions [*Palmer et al.*, 2003; *Millet et al.*, 2006]). On the other hand, an anthropogenic contribution to the HCHO column may be apparent at finer scales around urban areas; we return to this question below. Strong Ω_{HCHO} enhancements are visible over the Yucatan Peninsula during April and May, reflecting extensive biomass burning in this region during the dry season [*Yokelson et al.*, 2009].

[24] The observed HCHO distribution contrasts with that of NO_2, which is dominated by anthropogenic emissions over the continental United States [*Hudman et al.*, 2007]. Figure 6 illustrates this contrast, showing OMI Ω_{HCHO} and Ω_{NO2} for June-August during 2005–2007 (9 months total) binned by population density over four quadrants of the United States (25°–50°N, 65°–130°W, sectioned at 98°W and 38°N) (OMI NO_2 data provided by KNMI in collaboration with NASA, http://www.temis.nl/; population data sourced from 2005 Gridded Population of the World v.3, CIESIN/SEDAC, Columbia University, http://sedac.ciesin.columbia.edu/gpw/). The OMI data shown in Figure 6 are first gridded to 0.25° × 0.25° and then binned such that the mean population density changes by approximately a factor of 2 between bins. Employing population- and land area-weighted schemes (plots not shown), in which each bin represents equal land area or an equal fraction of the total population, produces similar results. The total number of OMI observations averaged in each bin in Figure 6 varies (10th–90th percentile) from 9,602 to 135,292 (median = 46,855) and the resulting uncertainty (standard error) varies (10th–90th percentile) from 3.2×10^{13} to 1.3×10^{14} molecules cm^{-2} (median = 5.75×10^{13} molecules cm^{-2}).

[25] For each U.S. quadrant in Figure 6, Ω_{NO2} increases strongly in the most densely populated areas, but in general this is not the case for Ω_{HCHO}. For instance, in the U.S. Southwest and Northwest, median Ω_{NO2} increases by more than a factor of 4 from remote to urban areas (first and last bins in Figure 6)

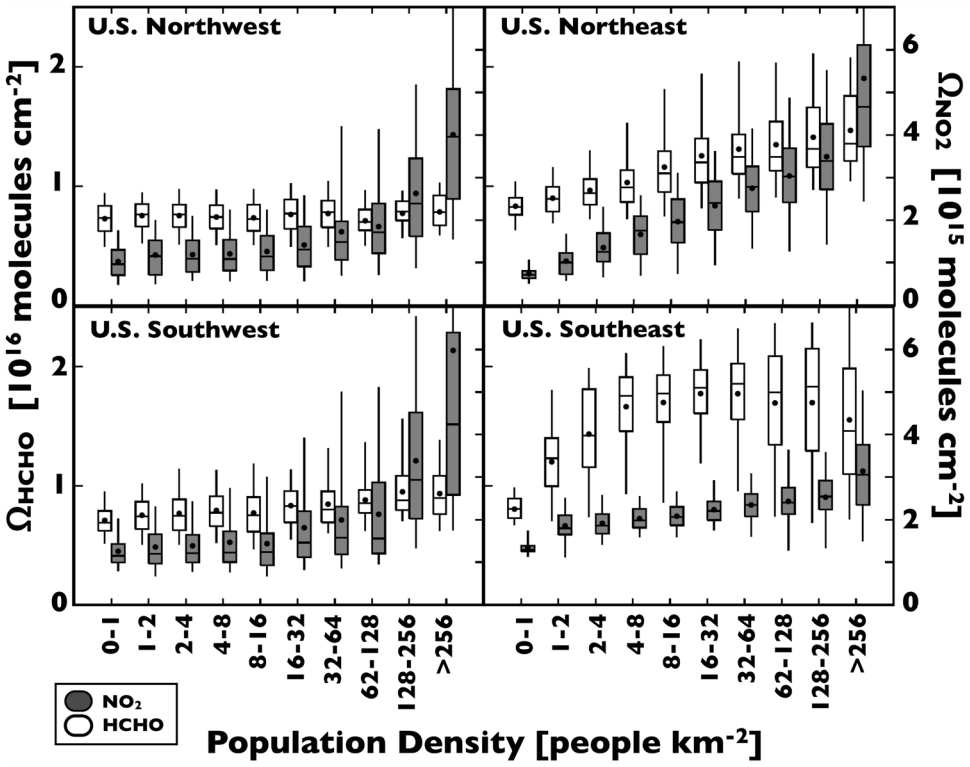

Figure 6. OMI HCHO and NO_2 columns over four quadrants of the United States (sectioned at 98°W, 38°N) as a function of population density. Summer months (June, July, August) from 3 years (2005–2007) are averaged together and ordered such that mean population density increases by approximately a factor of 2 between bins. Boxes show the interquartile range of column values; whiskers show the 5th and 95th percentiles. Interior dots and lines show the bin mean and median values, respectively. Note the different scaling for HCHO and NO_2.

while Ω_{HCHO} changes by <15%. Only in the U.S. Northeast (and perhaps the Southwest) does Ω_{HCHO} exhibit a discernable increase in densely populated areas. The stronger relationship between Ω_{HCHO} and population density for the U.S. Northeast may reflect the fact that this quadrant contains nearly half the U.S. population (45% of the population total, versus 27%, 19% and 9% for the Southeast, Southwest and Northwest, respectively), and the higher associated anthropogenic VOC emissions. On the other hand, the population distribution is biased to the southern part of this quadrant, so that temperature also increases with population density here (not shown). The observed Ω_{HCHO} trend may therefore reflect an underlying temperature-isoprene correlation. In any case, even in the Northeast the relationship between Ω_{HCHO} and population density is much weaker than for NO_2; median Ω_{HCHO} increases on average 7% between bins versus 25% for Ω_{NO2}.

[26] As in Figure 5, we see in Figure 6 that the western regions lack the broad HCHO enhancements seen in the eastern United States, with the highest Ω_{HCHO} values in the U.S. Southeast owing to strong regional isoprene emissions. This region also exhibits the weakest relationship between Ω_{NO2} and population density. This may reflect higher regional OH (due to high water vapor concentrations and actinic fluxes) and therefore shorter NO_2 lifetime, or it may reflect the population distribution within the region. We return to this point below in the context of HCHO. Finally, the anomalously low column values for HCHO and NO_2 in the first and second bins for this quadrant reflect low-population grid squares straddling the Gulf of Mexico coastline in Louisiana, Texas and Florida which are influenced by clean marine air.

[27] Figure 6 illustrates broad differences between HCHO and NO_2 column amounts in urban versus rural locations in the United States, but does not resolve any geographic biases that might exist within quadrant (for instance, populations predominantly on coasts versus inland). To examine urban-rural differences in more detail, and to assess the extent to which anthropogenic contributions to Ω_{HCHO} are detectable from the satellite, we plot Ω_{HCHO} in Figure 7 as a function of radial distance from the city center (population density-weighted city centroid) for selected major cities within each of the four U.S. quadrants. Data shown are averaged by season for 2005–2007 (inclusive) and show only HCHO column measurements over land. Ordinate scales in Figure 7 vary by quadrant to provide better resolution.

[28] The extent to which urban areas make a discernable contribution to Ω_{HCHO} variability over the United States via oxidation of reactive anthropogenic VOCs should manifest in Figure 7 as elevated Ω_{HCHO} values over the city, decreasing with distance from the city center. Relatively long-lived anthropogenic VOCs can also react to produce HCHO, but this contribution is spread out spatially and does not contribute to detectable variation from the perspective of the satellite instrument [*Palmer et al.*, 2003].

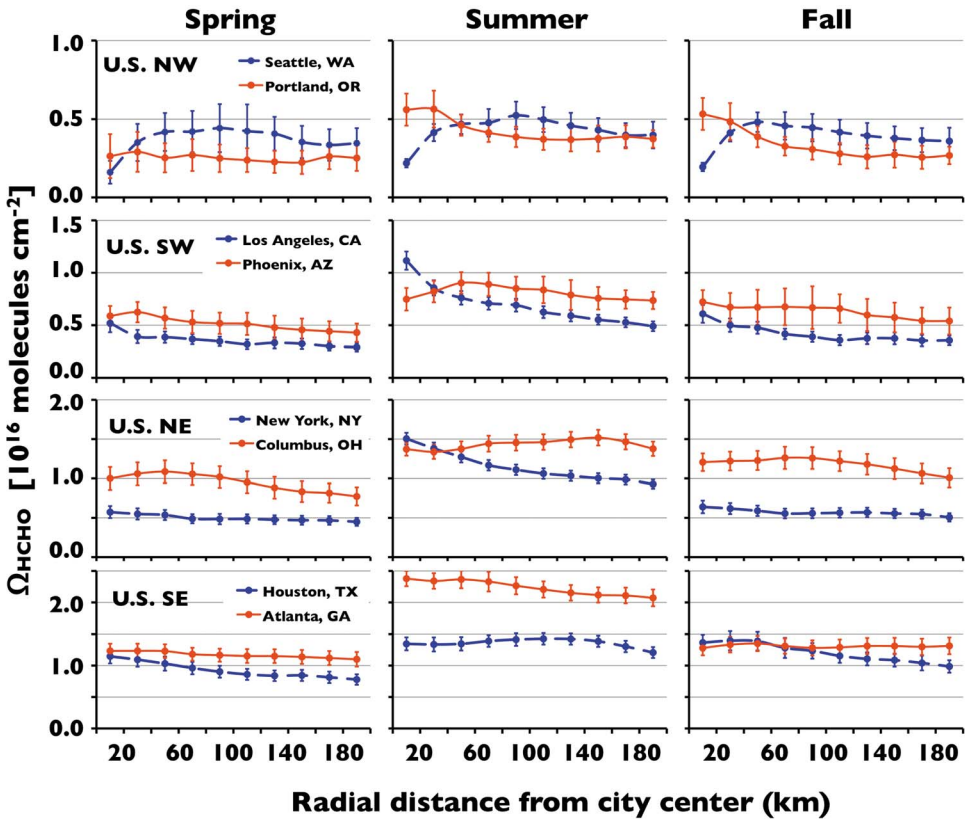

Figure 7. Seasonal mean OMI Ω_{HCHO} (spring is April–May; summer is June–August; fall is September–October) during 2005–2007 (inclusive) as a function of radial distance from city center. Data are plotted as mean values over 20 km intervals for eight major U.S. cities. Error bars show the standard error of OMI pixels included in each data point. Note the different vertical scale for each region.

Figure 7 reveals such gradients (high Ω_{HCHO} near the city center, low farther away) for some but not all cities, influenced by season and the local geography. In all seasons (most notably in summer) Los Angeles and New York stand out as the strongest examples of elevated Ω_{HCHO} in the city, compared to surrounding areas. During summer months, HCHO columns over the center of Los Angeles and New York are on average 128% and 67% higher than they are 200 km away, respectively.

[29] The strength of the anthropogenic signal for each city in Figure 7 depends in part on regional HCHO levels and therefore on regional biogenic isoprene emissions. For example, over Atlanta during summer, Ω_{HCHO} declines only weakly with distance from the city center, dropping by <13% over 200 km. However, rural Ω_{HCHO} values outside Atlanta are 2–4 times higher than outside New York or Los Angeles, masking any urban enhancement that might otherwise be detectable. Another factor attenuating the gradients in Figure 7 might be differing vegetation (cover and type) inside versus outside cities, resulting in lower isoprene emissions in urban than in rural environments.

[30] Portland exhibits the same general behavior as New York and Los Angeles, though to a lesser extent. Seattle is anomalous, with lower Ω_{HCHO} over the urban core compared to the surroundings; one likely explanation is inbound transport of clean marine air. Houston is also an interesting case, with elevated urban Ω_{HCHO} values during spring and fall (~30% higher in urban than in rural areas), but little or no apparent gradient (10% or less) during summer. Houston has high reactive olefin emissions from the local petrochemical industry [*Jobson et al.*, 2004; *Leuchner and Rappenglück*, 2010] (centered around the Houston ship channel, ~60 km from the Houston city center), but their summertime contribution to HCHO columns may be obscured in Figure 7 by increased isoprene emissions from the surrounding areas.

[31] Figure 8 shows the seasonality of OMI Ω_{HCHO} observations over the same eight cities shown in Figure 7, in comparison with terrestrial and oceanic background levels. Mean Ω_{HCHO} values for specific cities are determined as a built area-weighted average of OMI Ω_{HCHO} values within 100 km of each city's center (population density-weighted centroid). Terrestrial background Ω_{HCHO} values are determined for each U.S. quadrant as an average of all 0.25° grid squares in the region with ≤1% built area (comprising 77%, 48%, 73% and 37% of the land area in the U.S. Northwest, Northeast, Southwest and Southeast regions, respectively). Northern Hemispheric (0°–64°N) ocean background is determined as an average Ω_{HCHO} over marine grid squares.

[32] We see in Figure 8 that the urban HCHO columns tend to exhibit similar seasonality and dynamic range as the nonurban terrestrial background levels within each region. In the West, urban HCHO columns are similar to marine background levels during fall and spring, and are elevated by only 23%–92% compared to the marine background in summer. In the East, urban HCHO levels are higher during

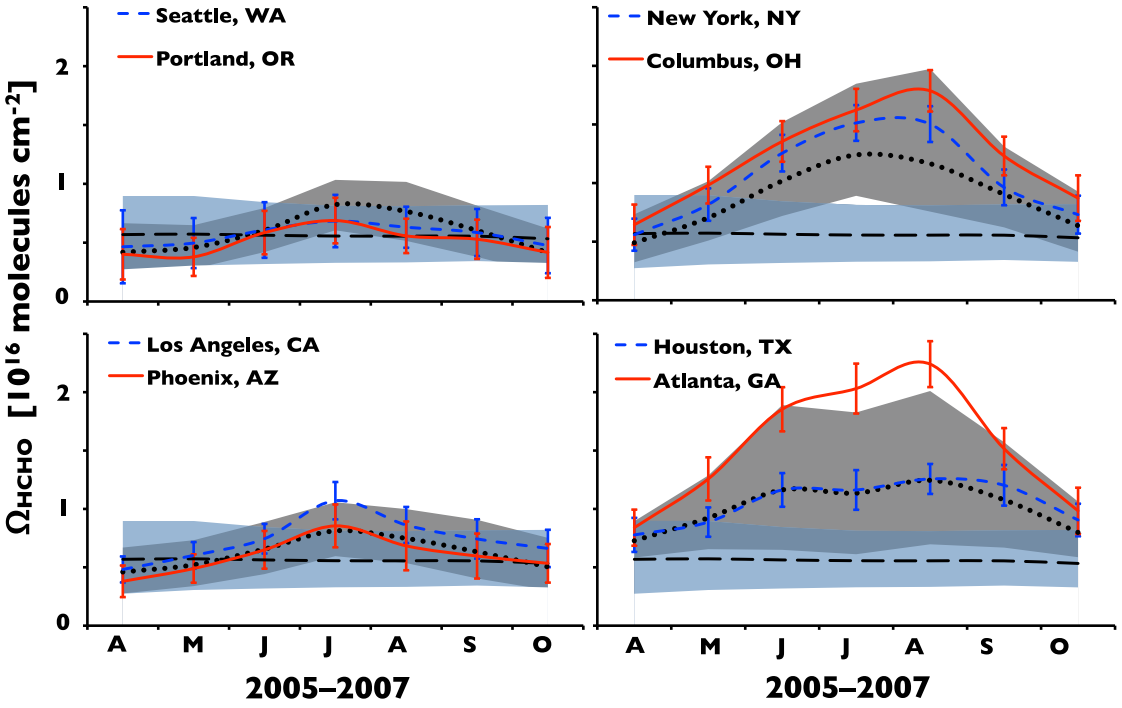

Figure 8. Seasonal urban Ω_{HCHO} (monthly averages for April–October during 2005–2007) over eight major U.S. cities, shown in their respective U.S. quadrants (sectioned at 98°W, 38°N). Data represent monthly built-area-weighted means with error bars showing the standard error of the gridded OMI data. The dotted black line and shaded area show the mean and 10th–90th percentiles of terrestrial background Ω_{HCHO} for each region, respectively. The dashed black and shaded blue areas show the mean and 10th–90th percentiles of Northern Hemisphere oceanic Ω_{HCHO} values (bounded by 0°–64°N).

summer, but still fall within the terrestrial background range seen within the quadrant (Atlanta lies outside the 0.1–0.9 background quantiles plotted in Figure 8, but inside the full range). In general, the seasonality in urban Ω_{HCHO} is consistent with that seen in the surrounding nonurbanized region. We examined a range of other major U.S. cities with comparable results.

6. Discussion

[33] Formaldehyde column (Ω_{HCHO}) measurements from the Ozone Monitoring Instrument (OMI), with 13 × 24 km^2 nadir footprint and daily global coverage, provide a highly resolved data set for examining biogenic and anthropogenic sources of VOCs. Here we used vertical profile measurements of HCHO from recent aircraft missions, combined with a global 3-D model (GEOS-Chem), to evaluate OMI HCHO retrievals and their fidelity in terms of resolving urban versus background HCHO column abundance. The average bias in the OMI columns was <3% relative to the aircraft values for the full data set, and −17% where $\Omega_{HCHO} > 5 \times 10^{15}$ molecules cm^{-2}. The −17% bias is within the expected uncertainty for space-borne HCHO retrievals, but may also reflect the aircrafts' preferential sampling of polluted plumes, which are averaged over the satellite footprint. This level of error is also similar to the uncertainty we expect for extrapolating in situ measurements to full HCHO columns. Further evaluation would be useful to determine the extent to which the discrepancy reflects retrieval bias rather than just representation error for this particular case. We discuss this issue further below.

[34] On average, GEOS-Chem reproduces the shape of the HCHO vertical profiles measured onboard the aircraft. The use of measured HCHO shape factors (normalized vertical profile) in the AMF computation did not improve the level of agreement with the aircraft data compared to using shape factors from GEOS-Chem, despite the 2° × 2.5° model resolution and urban focus of several of the flights. On this basis, we conclude that use of shape factors from a global model does not introduce a significant bias in satellite measurements of HCHO over urban areas.

[35] OMI Ω_{HCHO} correlates well with columns extrapolated from the aircraft profiles and with those derived from GEOS-Chem sampled along the flight tracks (R = 0.80 and 0.81). This finding suggests OMI and similar instruments reliably capture horizontal gradients in HCHO given sufficient averaging over time and/or space to reduce random noise in the retrieval.

[36] HCHO columns measured by OMI over North America and the Pacific exhibit temporal and spatial patterns consistent with biogenic VOCs as the dominant cause of variability, as has been demonstrated previously [*Abbot et al.*, 2003; *Martin et al.*, 2004a; *Millet et al.*, 2006; *Shim et al.*, 2005]. HCHO columns over urban areas generally exhibit similar seasonality as the nonurban terrestrial background for the surrounding region. However, fine-scale spatial gradients are detectable in the vicinity of certain urban areas, for instance in New York and Los Angeles, where Ω_{HCHO} can

decrease by >50% between the urban core and locations 200 km from the city. While detectable, in an absolute sense these gradients are much smaller than those associated with spatial and temporal changes in biogenic isoprene emission over the United States.

[37] While OMI and similar satellite sensors provide a rich global data set for understanding hydrocarbon emissions and chemistry, the scarcity of in situ HCHO measurements for coincident validation remains an issue. One way to address this would be a ground-based remote sensing network spanning urban to forested locales. This would provide a complementary data stream with high sensitivity to trace gases in the planetary boundary layer, and a means to cross-compare the current generation of satellite sensors and the upcoming GEO-CAPE instrumentation.

[38] **Acknowledgments.** This work was supported by the University of Minnesota, NASA (NNX10AG65G), and NSF (0853467). We thank NASA, KNMI, and SEDAC/CIESIN for data collection and processing and the INTEX-B, MILAGRO, and TexAQS II science teams.

References

Abbot, D. S., P. I. Palmer, R. V. Martin, K. V. Chance, D. J. Jacob, and A. Guenther (2003), Seasonal and interannual variability of North American isoprene emissions as determined by formaldehyde column measurements from space, *Geophys. Res. Lett.*, *30*(17), 1886, doi:10.1029/2003GL017336.

Barkley, M. P., P. I. Palmer, U. Kuhn, J. Kesselmeier, K. Chance, T. P. Kurosu, R. V. Martin, D. Helmig, and A. Guenther (2008), Net ecosystem fluxes of isoprene over tropical South America inferred from Global Ozone Monitoring Experiment (GOME) observations of HCHO columns, *J. Geophys. Res.*, *113*, D20304, doi:10.1029/2008JD009863.

Bey, I., D. J. Jacob, R. M. Yantosca, J. A. Logan, B. D. Field, A. M. Fiore, Q. Li, H. Y. Liu, L. J. Mickley, and M. G. Schultz (2001), Global modeling of tropospheric chemistry with assimilated meteorology: Model description and evaluation, *J. Geophys. Res.*, *106*, 23,073–23,095, doi:10.1029/2001JD000807.

Bovensmann, H., J. P. Burrows, M. Buchwitz, J. Frerick, S. Noël, V. V. Rozanov, K. V. Chance, and A. P. H. Goede (1999), SCIAMACHY: Mission objectives and measurement modes, *J. Atmos. Sci.*, *56*, 127–150, doi:10.1175/1520-0469(1999)056<0127:SMOAMM>2.0.CO;2.

Burrows, J. P., E. Hölzle, A. P. H. Goede, H. Visser, and W. Fricke (1995), SCIAMACHY—Scanning imaging absorption spectrometer for atmospheric chartography, *Acta Astronaut.*, *35*, 445–451, doi:10.1016/0094-5765(94)00278-T.

Burrows, J. P., et al. (1999), The Global Ozone Monitoring Experiment (GOME): Mission concept and first scientific results, *J. Atmos. Sci.*, *56*, 151–175, doi:10.1175/1520-0469(1999)056<0151:TGOMEG>2.0.CO;2.

Callies, J., E. Corpaccioli, M. Eisinger, A. Hahne, and A. Lefebvre (2000), GOME-2: Metop's second generation sensor for operational ozone monitoring, *ESA Bull.*, *102*, 28–36.

Chance, K., P. I. Palmer, R. J. D. Spurr, R. V. Martin, T. P. Kurosu, and D. J. Jacob (2000), Satellite observations of formaldehyde over North America from GOME, *Geophys. Res. Lett.*, *27*, 3461–3464, doi:10.1029/2000GL011857.

Curci, G., P. I. Palmer, T. P. Kurosu, K. Chance, and G. Visconti (2010), Estimating European volatile organic compound emissions using satellite observations of formaldehyde from the Ozone Monitoring Instrument, *Atmos. Chem. Phys.*, *10*, 11,501–11,517, doi:10.5194/acp-10-11501-2010.

Dufour, G., F. Wittrock, M. Camredon, M. Beekmann, A. Richter, B. Aumont, and J. P. Burrows (2009), SCIAMACHY formaldehyde observations: Constraint for isoprene emission estimates over Europe?, *Atmos. Chem. Phys.*, *9*, 1647–1664, doi:10.5194/acp-9-1647-2009.

Duncan, B. N., et al. (2010), Application of OMI observations to a space-based indicator of NO_X and VOC controls on surface ozone formation, *Atmos. Environ.*, *44*, 2213–2223, doi:10.1016/j.atmosenv.2010.03.010.

Fu, T.-M., D. J. Jacob, P. I. Palmer, K. Chance, Y. X. Wang, B. Barletta, D. R. Blake, J. C. Stanton, and M. J. Pilling (2007), Space-based formaldehyde measurements as constraints on volatile organic compound emissions in East and South Asia and implications for ozone, *J. Geophys. Res.*, *112*, D06312, doi:10.1029/2006JD007853.

Garcia, A. R., R. Volkamer, L. T. Molina, M. J. Molina, J. Samuelson, J. Mellqvist, B. Galle, S. C. Herndon, and C. E. Kolb (2006), Separation of emitted and photochemical formaldehyde in Mexico City using a statistical analysis and a new pair of gas-phase tracers, *Atmos. Chem. Phys.*, *6*, 4545–4557, doi:10.5194/acp-6-4545-2006.

Hudman, R. C., et al. (2007), Surface and lightning sources of nitrogen oxides over the United States: Magnitudes, chemical evolution, and outflow, *J. Geophys. Res.*, *112*, D12S05, doi:10.1029/2006JD007912.

Janson, R., C. De Serves, and R. Romero (1999), Emission of isoprene and carbonyl compounds from a boreal forest and wetland in Sweden, *Agric. For. Meteorol.*, *98–99*, 671–681, doi:10.1016/S0168-1923(99)00134-3.

Jobson, B. T., C. M. Berkowitz, W. C. Kuster, P. D. Goldan, E. J. Williams, F. C. Fesenfeld, E. C. Apel, T. Karl, W. A. Lonneman, and D. Riemer (2004), Hydrocarbon source signatures in Houston, Texas: Influence of the petrochemical industry, *J. Geophys. Res.*, *109*, D24305, doi:10.1029/2004JD004887.

Kesselmeier, J., and M. Staudt (1999), Biogenic volatile organic compounds (VOC): An overview on emission, physiology and ecology, *J. Atmos. Chem.*, *33*, 23–88, doi:10.1023/A:1006127516791.

Kurosu, T. P. (2008), OMHCHO readme file, Harvard-Smithsonian Cent. for Astrophys., Cambridge, Mass. (Available at https://www.cfa.harvard.edu/~tkurosu/SatelliteInstruments/OMI/PGEReleases/READMEs/OMHCHO_README.pdf.)

Ladstätter-Weißenmayer, A., J. Heland, R. Kormann, R. von Kuhlmann, M. G. Lawrence, J. Meyer-Arnek, A. Richter, F. Wittrock, H. Ziereis, and J. P. Burrows (2003), Transport and build-up of tropospheric trace gases during the MINOS campaign: Comparison of GOME, in situ aircraft measurements and MATCH-MPIC-data, *Atmos. Chem. Phys.*, *3*, 1887–1902, doi:10.5194/acp-3-1887-2003.

Leuchner, M., and B. Rappenglück (2010), VOC source-receptor relationships in Houston during TexAQS-II, *Atmos. Environ.*, *44*, 4056–4067, doi:10.1016/j.atmosenv.2009.02.029.

Levelt, P. F., G. H. J. van den Oord, M. R. Dobber, A. Malkki, H. Visser, J. de Vries, P. Stammes, J. O. V. Lundell, and H. Saari (2006), The ozone monitoring instrument, *IEEE Trans. Geosci. Remote Sens.*, *44*(5), 1093, doi:10.1109/TGRS.2006.872333.

Martin, R. S., I. Villanueva, J. Zhang, and C. J. Popp (1999), Nonmethane hydrocarbon, monocarboxylic acid, and low molecular weight aldehyde and ketone emissions from vegetation in central New Mexico, *Environ. Sci. Technol.*, *33*, 2186–2192, doi:10.1021/es980468q.

Martin, R. V., D. D. Parrish, T. B. Ryerson, D. K. Nicks Jr., K. Chance, T. P. Kurosu, D. J. Jacob, E. D. Sturges, A. Fried, and B. P. Wert (2004a), Evaluation of GOME satellite measurements of tropospheric NO_2 and HCHO using regional data from aircraft campaigns in the southeastern United States, *J. Geophys. Res.*, *109*, D24307, doi:10.1029/2004JD004869.

Martin, R. V., A. M. Fiore, and A. Van Donkelaar (2004b), Space-based diagnosis of surface ozone sensitivity to anthropogenic emissions, *Geophys. Res. Lett.*, *31*, L06120, doi:10.1029/2004GL019416.

Millet, D. B., et al. (2006), Formaldehyde distribution over North America: Implications for satellite retrievals of formaldehyde columns and isoprene emission, *J. Geophys. Res.*, *111*, D24S02, doi:10.1029/2005JD006853.

Millet, D. B., D. J. Jacob, K. F. Boersma, T. Fu, T. P. Kurosu, K. V. Chance, C. L. Heald, and A. Guenther (2008), Spatial distribution of isoprene emissions from North America derived from formaldehyde column measurements by the OMI satellite sensor, *J. Geophys. Res.*, *113*, D02307, doi:10.1029/2007JD008950.

Millet, D. B., et al. (2010), Global atmospheric budget of acetaldehyde: 3-D model analysis and constraints from in-situ and satellite observations, *Atmos. Chem. Phys.*, *10*, 3405–3425, doi:10.5194/acp-10-3405-2010.

Molina, L. T., et al. (2010), An overview of the MILAGRO 2006 campaign: Mexico City emissions and their transport and transformation, *Atmos. Chem. Phys.*, *10*, 8697–8760, doi:10.5194/acp-10-8697-2010.

Palmer, P. I., D. J. Jacob, K. Chance, R. V. Martin, R. J. D. Spurr, T. P. Kurosu, I. Bey, R. Yantosca, A. Fiore, and Q. Li (2001), Air mass factor formulation for spectroscopic measurements from satellites: Application to formaldehyde retrievals from the Global Ozone Monitoring Experiment, *J. Geophys. Res.*, *106*, 14,539–14,550, doi:10.1029/2000JD900772.

Palmer, P. I., D. J. Jacob, A. M. Fiore, R. V. Martin, K. Chance, and T. P. Kurosu (2003), Mapping isoprene emissions over North America using formaldehyde column observations from space, *J. Geophys. Res.*, *108*(D6), 4180, doi:10.1029/2002JD002153.

Palmer, P. I., et al. (2006), Quantifying the seasonal and interannual variability of North American isoprene emissions using satellite observations of the formaldehyde column, *J. Geophys. Res.*, *111*, D12315, doi:10.1029/2005JD006689.

Palmer, P. I., M. P. Barkley, T. P. Kurosu, A. C. Lewis, J. E. Saxton, K. Chance, and L. V. Gatti (2007), Interpreting satellite column observations of formaldehyde over tropical South America, *Philos. Trans. R. Soc. A*, *365*, 1741–1751, doi:10.1098/rsta.2007.2042.

Park, R. J., D. J. Jacob, B. D. Field, R. M. Yantosca, and M. Chin (2004), Natural and transboundary pollution influences on sulfate-nitrate-ammonium aerosols in the United States: Implications for policy, *J. Geophys. Res.*, *109*, D15204, doi:10.1029/2003JD004473.

Parrish, D. D. (2006), Critical evaluation of U.S. on-road vehicle emission inventories, *Atmos. Environ.*, *40*, 2288–2300, doi:10.1016/j.atmosenv.2005.11.033.

Parrish, D. D., et al. (2009), Overview of the Second Texas Air Quality Study (TexAQS-II) and the Gulf of Mexico Atmospheric Composition and Climate Study (GoMACCS), *J. Geophys. Res.*, *114*, D00F13, doi:10.1029/2009JD011842.

Rappenglück, B., P. K. Dasgupta, M. Leuchner, Q. Li, and W. Luke (2010), Formaldehyde and its relation to CO, PAN, and SO_2 in the Houston-Galveston airshed, *Atmos. Chem. Phys.*, *10*, 2413–2424, doi:10.5194/acp-10-2413-2010.

Sander, S. P., et al. (2006), Chemical kinetics and photochemical data for use in atmospheric studies, *Rep. 06-2*, 523 pp., Jet Propul. Lab., Pasadena, Calif.

Seco, R., J. Peñuelas, and I. Filella (2007), Short-chain oxygenated VOCs: Emission and uptake by plants and atmospheric sources, sinks, and concentrations, *Atmos. Environ.*, *41*, 2477–2499, doi:10.1016/j.atmosenv.2006.11.029.

Shim, C., Y. Wang, Y. Choi, P. I. Palmer, D. S. Abbot, and K. Chance (2005), Constraining global isoprene emissions with Global Ozone Monitoring Experiment (GOME) formaldehyde column measurements, *J. Geophys. Res.*, *110*, D24301, doi:10.1029/2004JD005629.

Singh, H. B., W. H. Brune, J. H. Crawford, F. Flocke, and D. J. Jacob (2009), Chemistry and transport of pollution over the Gulf of Mexico and the Pacific: Spring 2006 INTEX-B campaign overview and first results, *Atmos. Chem. Phys.*, *9*, 2301–2318, doi:10.5194/acp-9-2301-2009.

Stammes, P. (2001), Spectral radiance modeling in the UV-visible range, in *IRS2000: Current Problems in Atmospheric Radiation*, edited by W. L. Smith and Y. M. Timofeyev, pp. 385–388, Deepak, Hampton, Va.

Stavrakou, T., J. F. Müller, I. De Smedt, M. Van Roozendael, G. R. van derWerf, L. Giglio, and A. Guenther (2009a), Global emissions of non-methane hydrocarbons deduced from SCIAMACHY formaldehyde columns through 2003–2006, *Atmos. Chem. Phys.*, *9*, 3663–3679, doi:10.5194/acp-9-3663-2009.

Stavrakou, T., J. F. Müller, I. De Smedt, M. Van Roozendael, G. R. van derWerf, L. Giglio, and A. Guenther (2009b), Evaluating the performance of pyrogenic and biogenic emission inventories against one decade of space-based formaldehyde columns, *Atmos. Chem. Phys.*, *9*, 1037–1060, doi:10.5194/acp-9-1037-2009.

Vigouroux, C., et al. (2009), Ground-based FTIR and MAX-DOAS observations of formaldehyde at Réunion Island and comparisons with satellite and model data, *Atmos. Chem. Phys.*, *9*, 9523–9544, doi:10.5194/acp-9-9523-2009.

Weibring, P., D. Richter, J. Walega, and A. Fried (2007), First demonstration of a high performance difference frequency spectrometer on airborne platforms, *Opt. Express*, *15*, 13,476–13,495, doi:10.1364/OE.15.013476.

Wittrock, F., A. Richter, H. Oetjen, J. P. Burrows, M. Kanakidou, S. Myriokefalitakis, R. Volkamer, S. Beirle, U. Platt, and T. Wagner (2006), Simultaneous global observations of glyoxal and formaldehyde from space, *Geophys. Res. Lett.*, *33*, L16804, doi:10.1029/2006GL026310.

Yokelson, R. J., et al. (2009), Emissions from biomass burning in the Yucatan, *Atmos. Chem. Phys.*, *9*, 5785–5812, doi:10.5194/acp-9-5785-2009.

S. Alvarez and B. Rappenglück, Department of Earth and Atmospheric Sciences, University of Houston, Houston, TX 77004, USA.

N. L. Boeke and J. D. Marshall, Department of Civil Engineering, University of Minnesota, Minneapolis, MN 55455, USA.

K. V. Chance and T. P. Kurosu, Atomic and Molecular Physics Division, Harvard-Smithsonian Center for Astrophysics, Cambridge, MA 02138, USA.

A. Fried, D. Richter, J. Walega, and P. Weibring, Earth Observing Laboratory, National Center for Atmospheric Research, Boulder, CO 80307, USA.

D. B. Millet, Department of Soil, Water, and Climate, University of Minnesota, St. Paul, MN 55108, USA. (dbm@umn.edu)